

Structure of carbohydrate-bound polynuclear iron oxyhydroxide nanoparticles in parenteral formulations

Dina S. Kudasheva^{a,b}, Jriuan Lai^{a,b,c}, Abraham Ulman^{a,b,c}, Mary K. Cowman^{a,b,*}

^a *Othmer Department of Chemical and Biological Sciences and Engineering, Polytechnic University, Six Metrotech Center, Brooklyn, NY 11201, USA*

^b *Herman F. Mark Polymer Research Institute, Polytechnic University, Six Metrotech Center, Brooklyn, NY 11201, USA*

^c *The NSF MRSEC for Polymers at Engineered Interfaces, Polytechnic University, Six Metrotech Center, Brooklyn, NY 11201, USA*

Received 21 January 2004; received in revised form 28 April 2004; accepted 11 June 2004

Available online 11 September 2004

Abstract

Intravenous iron therapy is used to treat anemia associated with chronic kidney disease. The chemical structures of parenteral iron agents have not been characterized in detail, and correlations between structure, efficiency of iron delivery, and toxicity via catalysis of oxygen-derived free radical creation remain to be established. In this study, two formulations of parenteral iron have been characterized by absorption spectroscopy, X-ray diffraction analysis (XRD), transmission electron microscopy (TEM), atomic force microscopy (AFM), and elemental analysis. The samples studied were Venofer® (Iron Sucrose Injection, USP) and Ferrlecit® (Sodium Ferric Gluconate in Sucrose Injection). The 250–800-nm absorption spectra and the XRD patterns showed that both formulations contain a mineral core composed of iron oxyhydroxide in the β -FeOOH mineral polymorph known as akaganeite. This was further confirmed for each formulation by imaging using TEM and AFM. The average core size for the nanoparticles, after dialysis to remove unbound or loosely bound carbohydrate, was approximately 3 ± 2 nm for the iron–sucrose, and approximately 2 ± 1 nm for the iron–gluconate. Each of the nanoparticles consists of a mineral core, surrounded by a layer of bound carbohydrate. The overall diameter of the average bead in the dialyzed preparations was approximately 7 ± 4 nm for the iron–sucrose, and 3 ± 1 nm for the iron–gluconate. Undialyzed preparations have particles with larger average sizes, depending on the extent of dilution of unbound and loosely bound carbohydrate. At a dilution corresponding to a final Fe concentration of 5 mg/mL, the average particle diameter in the iron–sucrose formulation was approximately 22 ± 9 nm, whereas that of the iron–gluconate formulation was approximately 12 ± 5 nm.

© 2004 Elsevier Inc. All rights reserved.

Keywords: Parenteral formulations; Iron oxyhydroxide; Iron–carbohydrate complex; AFM; Iron–sucrose injection; Sodium ferric gluconate; Akaganeite

1. Introduction

Parenteral iron formulations containing iron complexed to monosaccharides or disaccharides are among the products currently used for the treatment of anemia.

Yet, the chemical structures of these materials have not been characterized in detail, and correlations between structure and complex stability, efficiency of iron delivery, and toxicity via catalysis of oxygen-derived free radical creation remain to be established. This study represents a first step toward complete characterization of the structures of this subclass of modern therapeutic iron–carbohydrate compounds.

Iron(III) oxyhydroxide is formed in aqueous solutions by the dissolution of a suitable iron salt, such as ferric chloride, at low pH, followed by neutralization

* Corresponding author. Tel.: +1 718 260 3054; fax: +1 718 260 3125.

E-mail address: mcowman@poly.edu (M.K. Cowman).

or basification [1–3]. The aquated iron ions are hydrolyzed initially to the mononuclear iron hydroxides $\text{Fe}(\text{OH})(\text{H}_2\text{O})_5$ and $\text{Fe}(\text{OH})_2(\text{H}_2\text{O})_4$. Formation of $\text{Fe}(\text{OH})_3(\text{H}_2\text{O})_3$ leads to the growth of a polynuclear (containing multiple linked iron atoms) iron oxyhydroxide with the approximate composition FeOOH . This mineral is insoluble unless stabilized by the presence of a water-soluble chelating agent.

Carbohydrates can be appropriate chelating agents for the stabilization of iron oxyhydroxide nanoparticles in colloidal suspension. Certain low molecular mass neutral carbohydrates, such as sucrose [4], or fructose [5] present multiple hydroxyl groups in a suitable array to chelate iron, although the binding is inherently weak in neutral aqueous solution. Polymeric carbohydrates such as dextran may also be used to stabilize nanoparticles because they present a large number of hydroxyl groups, which can cooperatively chelate the surface of iron oxyhydroxide nanoparticles. For a neutral carbohydrate, the chelation to iron is enhanced at high pH, because the hydroxyl groups may become deprotonated, thus acquiring a negative charge, and interacting more strongly with the cationic iron ion [6]. At neutral pH, inherently anionic carbohydrates such as gluconate or partially oxidized polysaccharides are more effective nanoparticle stabilizers. In these cases, a carboxyl group provides the negative charge over a broad pH range. Its chelation to iron can also drive the deprotonation of nearby hydroxyl groups, further enhancing the complex stability [4,7].

The structures of complexes formed between iron nanoparticles and polysaccharides have been studied previously, because iron–dextran complexes [8,9] and iron–polymaltosate complexes [10–12] (where polymaltosate was the commercial name for partially hydrolysed and oxidized starch) have been used for decades in the treatment of anemia. In a number of cases, the nanoparticle cores have been identified as iron oxyhydroxide. X-ray diffraction data are most consistent with the akaganeite ($\beta\text{-FeOOH}$) polymorph (polymorphs are solids with the same chemical composition but different crystal structures) [13–18]. Ultraviolet–visible (UV–VIS) absorption spectroscopy [5,17–19] and Mössbauer spectroscopy [13–16,20] have shown the presence of octahedrally coordinated high-spin Fe(III) ions. Extended X-ray absorption fine structure (EXAFS) studies [14] confirm the coordination of iron by 6 oxygen atoms, at an Fe–O distance of 1.95 Å, and the location of a somewhat disordered shell of iron ions at a distance of about 3.05 Å. The iron oxyhydroxide crystallite dimensions estimated from the broadening of X-ray diffraction peaks are generally about 1–5 nm in diameter [9,14,17]. Electron microscopy has shown that the dimensions of the core (which may be larger than the size of the crystalline portion) can range from 3 nm diameter spheres [9] to ellipsoidal particles with dimensions of up to

5×34 nm [21]. The mineral core is stabilized by interactions with the polysaccharide, presumably through the hydroxyl and/or carboxyl groups of the carbohydrate units, the latter having been generated by partial oxidation of the polysaccharide. The overall particle size is highly dependent on the nature of the polysaccharide and the mode of complex formation. An older commercial iron–dextran complex had a reported overall diameter of about 12–13 nm [9], whereas iron complexes with κ -carrageenan are reported to form 25–50 nm aggregates of 10–20 nm particles [17,18]. The apparent complex molecular mass, based on elution position in gel permeation chromatography (GPC) chromatograms, may range from 72 kDa (InFed[®]) to 90 kDa (Imferon[®]) to 265 kDa (Dexferrum[®]).

Information about the structure of iron complexes with low molecular mass carbohydrates has been predominantly derived from studies of soluble mono- or di-nuclear iron complexes. Weakly stable mononuclear complexes are formed by carbohydrates with structures that allow at least three hydroxyl groups to interact simultaneously with a single iron ion. For example, sucrose or its component sugar fructose can bind iron weakly at neutral pH [4–6]. There is much less information about complexes containing polynuclear iron species complexed with monosaccharides or disaccharides. Studies of ferric fructose systems suggested that the fructose may serve primarily to coat iron-containing particles at neutral pH. Interestingly, when the pH is raised, the formation of a tetra-deprotonated sugar moiety was proposed to break down the polynuclear iron to the mononuclear ferric fructose complexes. It was also noted that gluconate, with its carboxyl group, was much more effective in breaking down the particles [5]. For iron sucrose, earlier studies suggest the presence of polynuclear iron complexed with sucrose, in which the mineral core has been proposed to be a 2-line ferrihydrite [22] rather than an iron oxyhydroxide.

Some of the questions that may arise in the analysis of polynuclear iron–carbohydrate complexes include: (1) the composition and polymorphic form and degree of crystallinity of the iron mineral component, (2) the size and shape of the nanoparticles, (3) the stability of the nanoparticles, (4) the location of the saccharide component within the particle, (5) the molar ratio of iron to saccharide, and (6) the mode of binding between the iron and saccharide components, including the extent of saccharide deprotonation in the complex. In the present work, we address some of these questions by examining two different iron–carbohydrate complexes with respect to the mineral environment of the iron, the nanoparticle size, and the particle stability upon dilution or separation from unbound carbohydrate by dialysis.

2. Materials and methods

The parenteral iron formulations used in this study were an iron–sucrose (Venofer[®], Iron Sucrose Injection, USP, lots 1644 and 2323A), from American Regent, Inc., Shirley, NY, and an iron–gluconate in sucrose (Ferrlecit[®], Sodium Ferric Gluconate Complex in Sucrose Injection, lots 1F541 and 1C239), from Watson Pharmaceuticals, Inc., Corona, CA. Venofer[®] was supplied as the iron–sucrose complex in 5 mL vials containing 100 mg of elemental iron in 30% sucrose solution (20 mg Fe/mL) at a pH of about 10.5–11.1. The apparent average molecular mass is stated in the package insert to be 34–60 kDa. Ferrlecit[®] was obtained as the iron–gluconate complex in 5 mL ampules containing 62.5 mg of elemental iron as a sodium salt of a ferric gluconate complex in 20% sucrose (12.5 mg Fe/mL) at a pH of about 7.7–9.7. The apparent average molecular mass is stated in the package insert to be 350 ± 23 kDa. Some samples, where noted in the text, were subjected to dialysis to remove low molecular mass components. Dialysis of samples for absorption spectroscopy was performed against deionized water, at a pH of about 5.4, in Slide-A-Lyzer Dialysis Cassettes (Pierce, Rockford, IL) made of low-binding regenerated cellulose membrane, molecular weight cutoff (MWCO) 10,000. Cassette capacity was 0.5–3 mL. Larger volumes of dialyzed samples were needed for AFM and TEM studies; in that case dialysis against deionized water at neutral pH, or with pH adjusted with KOH to match the sample pH, was performed in tubes made of Spectra/Por Molecularporous Regenerated Cellulose Membrane (Spectrum Laboratories Inc., Rancho Domingues, CA) with MWCO 6–8,000. Dialysis time for both trials was 20–48 h. Dialyzed samples were sent to Huffman Laboratories, Inc. (Golden, CO) for elemental analysis to determine the amount of iron, carbon and sodium.

Absorption spectra were recorded on a Perkin–Elmer Lambda 800 UV/VIS absorption spectrophotometer. The spectra were analyzed with UV WinLab software v3.00.03. The spectra were recorded in the range of 800–200 nm for original non-diluted samples and for diluted or dialyzed samples. This instrument has the ability to analyze samples with relatively high absorbance. Its photometric linearity at an absorbance (A) of 3 is ± 0.006 A units and at A of 2 is ± 0.002 A units. The photometric accuracy at A of 2 is ± 0.003 A units and stray light in the range of 220–370 nm is <0.00008% T. The photometric range is ± 7 A. For the undiluted samples, cylindrical quartz cells of path length 0.001 or 0.01 cm were employed; for all other samples a cylindrical quartz cell of path length 0.01 cm was used. The reference was water. All spectra were recorded as absorbance vs. wavelength of light in nm. Molar extinction coefficients were calculated from the absorbances at wavelengths of 300 and 470 nm, based

on the molar concentration of iron in each sample. The molar iron concentrations were calculated from the stated weight concentration of iron in each sample.

X-ray powder diffraction (XRD) patterns were recorded at a scanning rate of 0.008° min⁻¹ in the range 2θ from 0° to 70° using a Philips X-ray diffractometer with Cu Kα radiation (λ = 1.5418 Å). Original and dialyzed samples were prepared by freeze-drying prior to analysis. The average iron mineral crystallite size, *D*, was calculated from the observed XRD profiles using the peak full width at half maximum height (β) of the selected diffraction peak, using the Scherrer formula [23]:

$$D = K\lambda/\beta \cos \theta,$$

where *K* is the Scherrer constant, with a value of 0.94. For recorded crystalline patterns, diffraction angles and interplanar spacings obtained were compared with the values compiled in the JCPDS-ICDD (Joint Committee on Powder Diffraction Standard-International Center for Diffraction Data-copyright PSI International) reference cards.

Electron microscopic studies of the iron-core crystal size and morphology for the iron–carbohydrate samples were carried out by using a Phillips CM-12 Transmission Electron Microscope (100 keV). All preparations were deposited one night before imaging onto a carbon stabilized Formvar-coated copper grid (400 mesh), purchased from Ted Pella, Inc., Redding, CA. Approximate grid hole size is 42 μm, and the thickness of Formvar films stabilized with carbon is 5–10 nm. All attempts to image the original undiluted liquids were not successful, because the resulting film on a grid was too thick for electrons to penetrate. Consequently, the iron–carbohydrate complexes were dialyzed and the grid was dipped into the sample and then the excess liquid was removed with a very gentle flow of compressed nitrogen.

Atomic force microscopy (AFM) was used to determine size and shape of iron–carbohydrate complexes. The instrument used was a MultiMode Scanning Probe Microscope with Nanoscope IIIa controller and a type EV scanner (Veeco Instruments, Inc). The scanner was calibrated in the *x*–*y* plane using the 1 μm etched grid, and in the *z*-direction using the 200 nm height calibration standard. The samples for imaging were prepared in two ways. In the first procedure, samples were diluted 2 to 80-fold with deionized water prior to analysis. In the second procedure, samples were dialyzed against deionized water prior to analysis. In both cases, 4 μL of sample was put on a freshly cleaved mica surface, then after 20–30 s the surface was rinsed with 100 μL of deionized water to get rid of unbound particles, and the surface was dried by a gentle flow of nitrogen. The AFM imaging technique used was Tapping ModeTM. TESP etched silicon cantilever probes of 125 μm nominal length were used, at a drive frequency of approximately 240–280 kHz. We generally use an RMS (root

mean square) voltage of approximately 2.5–3 V, and adjust the setpoint for optimum image, which is generally about 1 V below the RMS voltage. Both height and amplitude information were recorded at a scan rate of 2–3 Hz, and stored in a 256×256 pixel format. Images were processed using the Nanoscope version 4.43r8 software. For optimum clarity in visual presentation of the nanoparticle images in the figures, flattening of first order was employed unless stated otherwise. For images to be used in measuring heights, the only image processing was zero order flattening. These images were analyzed to determine height and diameter of the particles observed. Although the height measurement is considered accurate, the apparent particle diameter is broadened by the finite dimensions of the probe tip. A correction for the tip broadening effect has been made following the procedure of Margeat et al. [24]. The apparent diameter measured at half height, S , is related to the real diameter, D , and the tip radius, R , according to the following equation [24]:

$$S = 2 \left(RD + \frac{D^2}{4} \right)^{1/2}$$

The tip radius was estimated by imaging DNA, which has a real chain diameter of 2 nm. For one AFM tip used, the measured apparent diameter of DNA at half height was 11.8 nm, resulting in an estimated tip radius of 16.8 nm. A second tip had an estimated radius of 14.8 nm. The appropriate tip radius was used to estimate corrected diameters in our images, although we may expect some minor variation for a given tip as a function of use. Thus the estimated particle diameters are subject to uncertainty on this basis. The relative diameters for a given series of samples differing in dilution were measured

on the same day and with a single tip, and should be representative of the effect of dilution on the particle diameter. The relative sizes of particles in different iron formulations were confirmed by analysis of all samples on the same day, using a single tip, and running a calibration image of DNA on the same occasion.

3. Results and discussion

3.1. Absorption spectroscopy

For Fe(III) in a high spin state octahedrally coordinated to oxygen, several characteristic absorption bands are expected. At 250–390 nm, a band of high intensity arises from oxo-metal charge transfer transitions, as has been reported for Fe(III)–glucose at 320 nm and for Fe(III)–sucrose at 370 nm [19]. Low intensity bands at 470–500 nm and 560–580 nm arise from d to d transitions of octahedral d^5 complexes of Fe(III). For low spin Fe(III), the latter bands would be of high intensity. The presence of Fe(II) would result in a band at 420–450 nm for the d–d transition of octahedral d^6 Fe(II), and a high intensity band at 800–900 nm for an aquated-Fe(II) complex [25].

The spectral shapes of the studied parenteral iron formulations show a weak absorption band at about 470–500 nm and a strong band about 300 nm. Fig. 1 shows the absorption spectra for the two samples after dilution to the same nominal concentration of 5 mg Fe/mL, to facilitate spectral shape comparison. The 470–500 nm band is attributed to the d–d transition of octahedral high spin d^5 Fe(III). The 300 nm band shows that the iron is chelated to oxygen, and is due to the oxo-metal

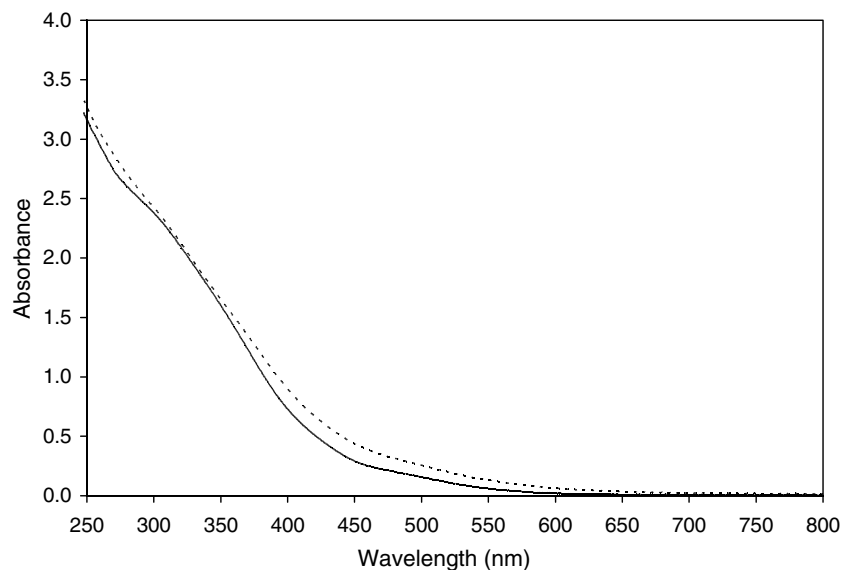


Fig. 1. Absorption spectra of iron–sucrose (dashed line), and iron–gluconate (solid line) diluted to nominal iron concentrations of 5 mg/mL and analyzed in an optical cell of 0.01 cm path length.

Table 1
Characterization of iron–carbohydrate complexes by absorption spectroscopy

Sample	Fe Conc. (mg/mL)	Cell path length (cm)	ϵ_{300} ($M^{-1} \text{ cm}^{-1}$)	ϵ_{470} ($M^{-1} \text{ cm}^{-1}$)	$\epsilon_{300}/\epsilon_{470}$
Iron–sucrose	20	0.001	2990		7.9
	20	0.01		380	
	5	0.01	2720	390	7.0
Iron–gluconate	12.5	0.001	2600		9.0
	12.5	0.01		290	
	5	0.01	2670	250	10.6

charge transfer absorption band. There is no evidence for the existence of low spin state Fe(III) or for aquated Fe(II). The shapes of the spectra are essentially the same for both iron–carbohydrate samples; both formulations showed characteristic absorption spectra expected for Fe(III) complexes in an octahedral d^5 high spin state.

The position of the d–d transition band around 500 nm has been shown to depend on the distance between two neighboring Fe atoms [26]. Thus, in the case of face-sharing octahedra of an iron oxide hematite, this band is above 500 nm. For the edge- and corner-sharing octahedra and hence larger Fe–Fe distances in iron oxyhydroxides this transition is weaker and lies at shorter wavelengths of 470–499 nm [27]. Based on the fact that both iron formulations have this band at approximately the same position, we can conclude that the nature of the iron core is the same and both spectra are compatible with the expected ferric oxyhydroxide mineral form.

The molar extinction coefficients of the absorption bands for each sample were closely similar (Table 1). The peak at 300 nm was best quantitated in undiluted samples analyzed in an optical cell with a path length of 0.001 cm. Calculated extinction coefficients at 300 nm were approximately 2600–3000 $M^{-1} \text{ cm}^{-1}$ for the two samples. This compares with reported values of 6660 for a different iron–sucrose preparation [19] and 1700 for iron–carrageenan [17]. The shoulder at 470–

500 nm was best quantitated in undiluted sample analyzed in an optical cell with a 0.01 cm path length. The extinction coefficient at 470 nm was approximately 300–400 $M^{-1} \text{ cm}^{-1}$ for the two samples.

The stability of the iron core structure in each of the iron formulations was assessed by dilution and/or dialysis. Dilution to a concentration of 5 mg Fe/mL, or dialysis against water resulting in a similar dilution, had no significant effect on the spectral shape or molar extinction coefficients of the iron absorption bands (Table 1).

3.2. Transmission electron microscopy (TEM)

TEM micrographs of dialyzed iron–sucrose and dialyzed iron–gluconate samples at equivalent magnifications are compared in Fig. 2. The beadlike iron mineral cores appear to be fairly uniform in size for a given sample. This uniformity reflects the manufacturing processes, and results in particles with a narrow range of sizes. The comparison of the images of two samples shows that the iron–gluconate particles have cores that are generally slightly smaller (Fig. 2(a)) than those of iron–sucrose (Fig. 2(b)).

Measurement of the diameters of the electron dense particles is used to estimate the diameter of the iron mineral core in a given sample. For iron–sucrose, the results indicate a mineral core size distribution ranging from

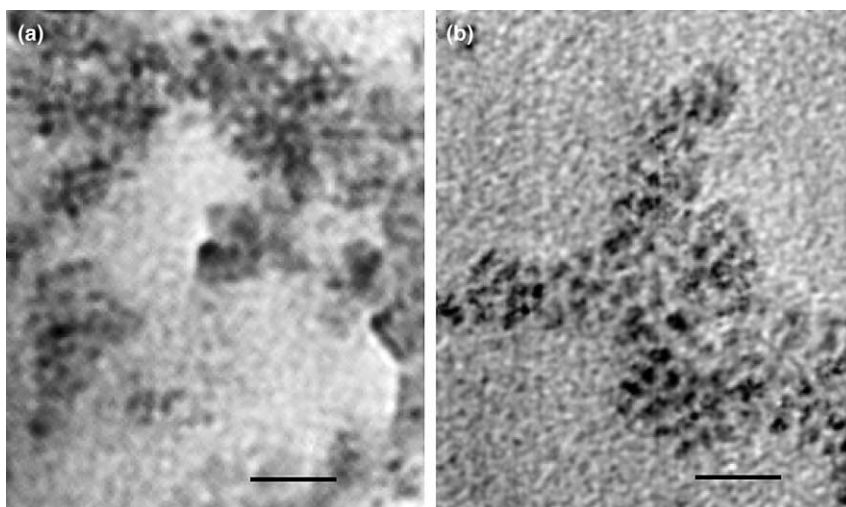


Fig. 2. Transmission electron microscopy image of (a) dialyzed iron–gluconate complex and (b) dialyzed iron–sucrose complex. The bar is 20 nm.

approximately 1.0–6.5 nm. The average size of the core is 3 ± 2 nm ($n = 20$). For iron–gluconate, the mineral core diameter ranges from approximately 0.9–3.5 nm, and the average diameter of the core is 2 ± 1 nm ($n = 20$).

3.3. X-ray powder diffraction

The chemical structure of the iron core was evaluated by means of X-ray diffraction (XRD) analysis. XRD is considered to be the most reliable way to identify a particular iron polymorph because it is based on the long range order of the atoms [3]. The diffractograms ob-

tained for lyophilized samples of original, nondialyzed preparations were compared with reference data for different iron oxyhydroxide mineral phases, similar in composition and structure (Table 2). Both iron–carbohydrate samples give a crystalline pattern of a single phase whose peak positions and intensities match with reported JSPDS-ICDD reference data for iron (III) oxyhydroxide akaganeite β -FeOOH. The X-ray results are not consistent with the ferrihydrite structure found in ferritin [28]. In addition, two peaks in the diffractograms of both samples in the small angle region (11.5° and 20°) belong to sucrose. From the analysis

Table 2

Interplanar spacings in Angstroms and relative strength of reflections (from JCPDS-ICDD cards for sucrose and iron minerals and from recorded diffractograms for original nondialyzed formulations)

Sucrose	Hematite	Goethite	Ferrihydrite	Akaganeite	Iron–sucrose (angle)	Iron–gluconate (angle)
7.58s					7.59 (11.5°)	7.54 (11.7°)
6.94m				7.467s		6.91 (13.1°)
6.73m				5.276m		
		4.98w			4.68 (17.1°)	
4.71s						
4.52s						
4.25m		4.18s				
	3.68m			3.728w		
3.59s					3.61 (22.3°)	3.61 (22.3°)
3.53m						
				3.333s		
2.88w						
	2.70s	2.69m				2.69 (33.3°)
		2.58w		2.634m	2.64 (33.5°)	
				2.550s	2.56 (35.1°)	2.555 (35.13°)
	2.52s		2.50s			
2.35m		2.45s		2.356w		2.35 (38.2°)
2.339w				2.295m	2.34 (38.3°)	
					2.28 (39.6°)	
2.028w	2.21m	2.25w	2.21s			
1.971w		2.19m		1.954m		
	1.84m		1.96s			
		1.72m	1.72m	1.755w	1.76 (51.8°)	1.75 (52.01°)
	1.69s			1.643m	1.64 (55.5°)	1.66 (55.2°)
				1.515w	1.52 (61.1°)	
			1.51m	1.503w		1.50 (61.8°)
	1.49m			1.489w	1.49 (62.3°)	1.49 (62.3°)
			1.48s	1.485w		
	1.45m			1.445m		
		1.42w				
		1.393w				
		1.36w				
		1.345w				
		1.317w				
		1.29w				
	1.055w					
	1.033w					
	0.960w					
	0.9581w					
	0.8436w					

s, strong; m, medium; and w, weak.

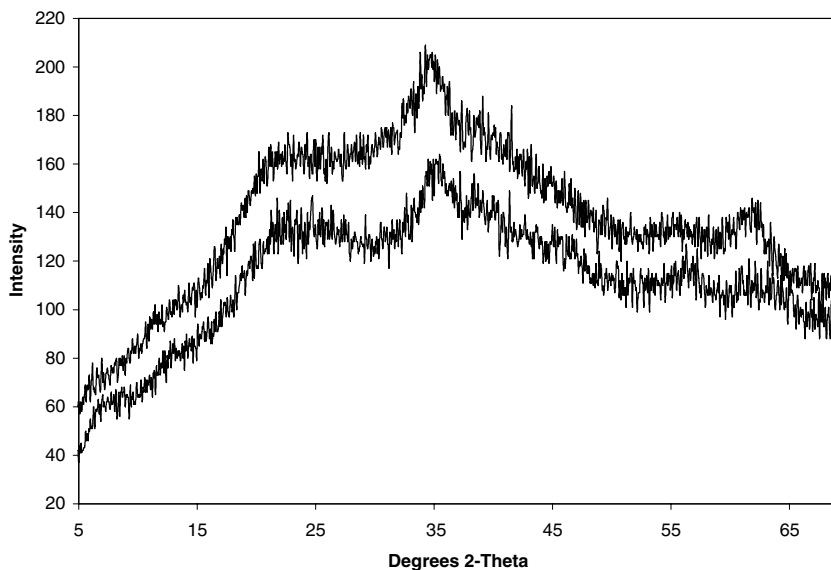


Fig. 3. XRD patterns of iron-sucrose (top) and iron-gluconate (bottom).

of the diffractograms in Fig. 3, it can be also concluded that all peaks broadened evenly, without the presence of a selective peak broadening, i.e., there was no preferential deformation plane due to the complexation with sucrose or gluconate.

It should be mentioned that XRD patterns of both formulations appear to have a very weak diffraction peak from the (002) plane (diffraction angle $2\theta = 61.15^\circ$), which would indicate the presence of Cl^- anions. The presence of Cl^- is in accord with the tunnel-containing akaganeite structure.

On the XRD pattern of iron-sucrose sample after pH-matched dialysis, the sucrose peaks at 11.5° and 22° are almost eliminated (Fig. 4, top spectrum). How-

ever, an overall lifting of the area of their presence around 20° confirms that there is still some sucrose in the sample and that the sucrose is not uniformly ordered. Dialysis did not destroy the iron mineral core, since the main reflection attributed to the akaganeite polymorph remains strong after dialysis.

For iron-gluconate, the effect of removing unbound sucrose was more noticeable (Fig. 4, bottom spectrum). In addition to the apparent disappearance of the sucrose peaks at 11.5° and 22° , the pattern of the dialyzed sample has a newly visible akaganeite peak at 26.8° . That difference in the peak appearance between the two dialyzed samples occurs despite the fact that the size of the iron-gluconate core is slightly smaller than that of

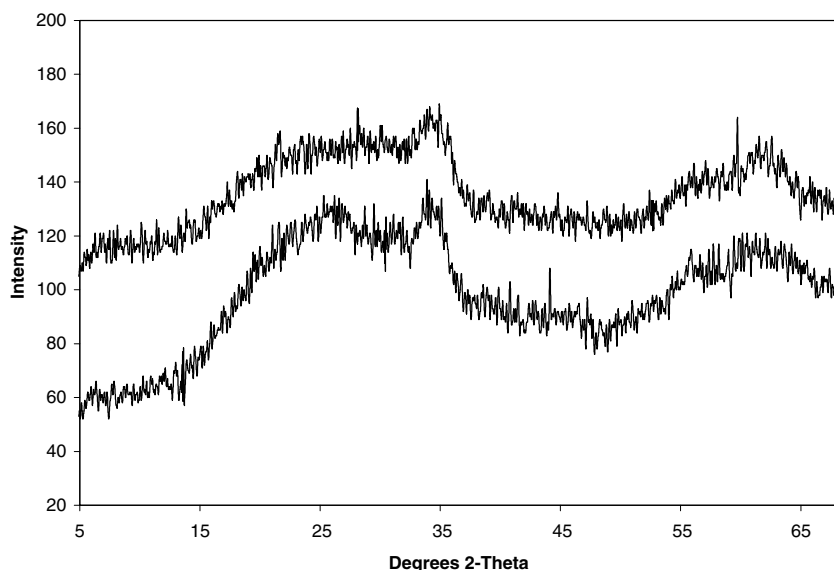


Fig. 4. XRD patterns of dialyzed iron-sucrose (top) and dialyzed iron-gluconate (bottom).

iron–sucrose, as demonstrated by TEM. On the basis of overall core size, the peaks in the XRD pattern of iron–gluconate should be less pronounced. Thus, the difference in the diffractogram appearance may indicate more uniform crystallites in the iron–gluconate than in the iron–sucrose, after dialysis to remove unbound and loosely bound carbohydrate.

Our FTIR studies (unpublished data) of different iron oxyhydroxide polymorphs also confirmed that the iron core of both formulations has the chemical structure of iron (III) oxyhydroxide akaganeite β -FeOOH.

The average crystallite size, D , was estimated from the diffraction peak from the (211) plane (diffraction angle $2\theta = 35.1^\circ$), and gave a similar result for both formulations. In the case of nondialyzed samples, the crystallite size for iron–sucrose was estimated to be 4.6 nm, while for iron gluconate it was 4.1 nm. For the iron–sucrose sample after pH-adjusted dialysis (Fig. 4), D calculated for the same peak gave a smaller size of 3.4 nm. The average crystallite size for the dialyzed iron–gluconate was 3.5 nm. These values are slightly higher than the core diameters estimated for dialyzed samples by transmission electron microscopy. Considering the difficulty in accurately measuring the diffraction peak width at half height, the TEM data are considered more reliable.

3.4. Atomic force microscopy

Imaging the iron–carbohydrate complexes was performed for samples applied to a mica surface, followed by brief rinsing to remove unbound material, including excess soluble low molecular mass carbohydrates. The images of the two iron formulations showed large numbers of beadlike nanoparticles spread over the scanning surface.

The arrangement of particles on the mica surface is different from the arrangement on the surface of the TEM grid, which is quite expected because the surfaces are different. AFM mica is hydrophilic, whereas the TEM grid is covered with carbon, which makes it highly hydrophobic. Thus the particles are more uniformly distributed on the mica surface than on the carbon coated TEM grid.

Fig. 5 shows $3\ \mu\text{m} \times 3\ \mu\text{m}$ scans of each iron formulation sample at an iron concentration of 5 mg/mL. The surfaces showed residual excess sucrose or sucrose and gluconate surrounding the nanoparticles. The beadlike particles, which include both the mineral core and the bound carbohydrate, appear to be similar in size for iron–sucrose and iron–gluconate.

Images obtained at higher resolution are preferred for more accurate measurements of the nanoparticle sizes. Fig. 6 shows $1\ \mu\text{m} \times 1\ \mu\text{m}$ scans of nanoparticles from each preparation type, analyzed at comparable iron concentrations after dilution with water. The distributions

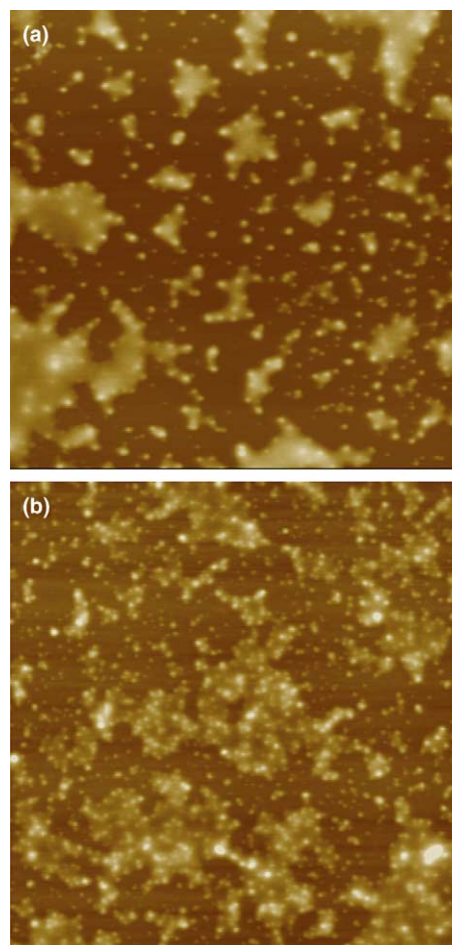


Fig. 5. Atomic force microscope height images of: (a) iron–sucrose complex, (b) iron–gluconate complex in sucrose, after dilution to an iron concentration of 5 mg/mL. Image size $3\ \mu\text{m} \times 3\ \mu\text{m}$, with a color scale covering a height range of 15–20 nm (darker features being lower in height than lighter ones).

of particle heights measured from the images in Fig. 6 are given in Table 3 for iron–sucrose and Table 4 for iron–gluconate. An equal number of particles (75) were analyzed at each concentration for each preparation type.

At a concentration of about 5 mg Fe/mL, the iron–sucrose complexes (Fig. 6(a) and Table 3) appear as beads with an average height of about 3.5 nm, and a corrected width of approximately 22 nm. Analyzed at the same 5 mg Fe/mL concentration, the iron–gluconate in sucrose complex (Fig. 6(e) and Table 4) had an average height of approximately 3.1 nm, and an average apparent particle width of approximately 12 nm.

For an incompressible spherical bead, the height and width measurements should both be equal to the bead diameter. Two factors contribute to the mismatch between vertically measured height and horizontally measured diameter. The first is a flattening effect caused by the tapping impact of the probe. The carbohydrate component of the beads is subject to compression and dis-

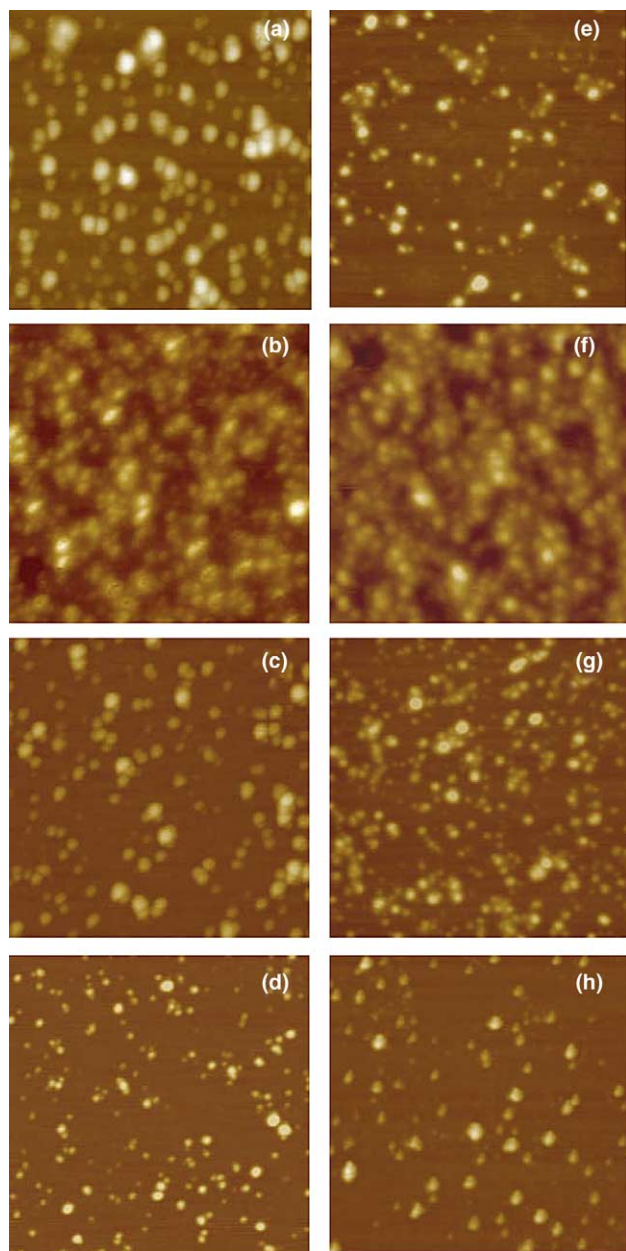


Fig. 6. Atomic force microscope height images of iron–sucrose complex (a–d), and iron–gluconate complex in sucrose (e–h) at various dilutions. Final iron concentrations are 5 mg/mL (top row), 2–2.5 mg/mL (row 2), 0.8–1.3 mg/mL (row 3), and 0.6–0.7 mg/mL (row 4). All image sizes $1\ \mu\text{m} \times 1\ \mu\text{m}$, with a color scale covering a height range 8–20 nm in different images.

placement in the vertical direction. In addition, the presence of residual unbound sucrose surrounding each bead on the surface can make the apparent bead diameter larger than the true diameter of the bead.

The effects of dilution and/or dialysis of the iron formulations on the measured particle sizes were investigated. The iron–sucrose sample showed a relatively modest reduction in height with dilution, but a significant decrease in apparent particle width. The initial decrease in average nanoparticle height from 3 to 2 nm,

observed upon dilution to 2 mg Fe/mL, was primarily caused by the fact that the particles were deeply embedded in a sucrose residue covering the surface for that particular sample (Fig. 6(b)). Thus, the measured height in that case is really only the height of the upper part of the particles above the sucrose. That phenomenon can also explain the observation that upon the next dilution to 0.8 mg/mL the average measured height increased again to 3 nm (Fig. 6(c)), in contrast with the logical expectation that upon dilution the particle size would decrease. Upon the final dilution to 0.66 mg/mL the average measured height stayed nearly constant at 3 nm. We conclude that the height of the particles is relatively stable with dilution. The fact that the average height of a whole iron–sucrose particle approximately coincides with the average diameter of the iron mineral core from TEM images indicates the severity of the carbohydrate shell compression and/or displacement by the AFM tip. The corrected iron–sucrose particle diameter, in contrast, decreased significantly from 22 nm at the highest concentration to approximately 6 nm at the lowest concentration. This latter measurement is least affected by unbound but loosely associated sucrose surrounding the beads on the surface. These results were reproduced in a second series of experiments (Table 3) comparing particle size at concentrations of 0.8 and 0.4 mg/mL. The iron–sucrose particles showed no difference in the particle height, but a significant decrease in diameter from 15 to 4 nm. The above observations might mean that dilution below about 0.8 mg/mL, which is a 25-fold dilution of original sample, results in a loosening of weakly bound sucrose. The average final particle size observed at the greatest dilution is therefore approximately 3 nm in height and 4–6 nm in diameter. A similar particle size is obtained for samples dialyzed against water at pH 10 to remove unbound or weakly bound carbohydrates. The dialyzed iron–sucrose particles showed an average height of 3 nm, and apparent width of 7 nm (Fig. 7(a) and Table 3), in good agreement with the dimensions of the particles analyzed at the greatest dilution.

The iron–gluconate particles in sucrose are affected by the same height and width measurement uncertainties as seen for iron–sucrose (Table 4). Dilution from 5 to 2.5 mg/mL results in an apparently significant reduction in height and increase in width. This is partially an artifactual change, resulting from a variable background elevation due to unbound or loosely bound sucrose and gluconate. Disregarding that data point, the particle height decreases only slightly, over the entire range of dilution from 5 to 0.62 mg/mL. The particle apparent width decreased from 12 to 11 nm.

Dialysis of the iron–gluconate formulation against water at pH 8 was effective in further removal of unbound or loosely bound carbohydrate. In three separate experiments, dialysis of iron–gluconate nanoparticles re-

Table 3
AFM measurements of iron–sucrose at different dilutions and after dialysis

Fe Concentration (mg/mL)	Height range (nm)	Average height (nm)	Diameter range (nm)	Average diameter (nm)
<i>Series 1</i>				
5.0 (<i>n</i> = 75)	0.8–8.8	4 ± 2	5.1–43.9	22 ± 9
2.0 (<i>n</i> = 75)	0.5–4.5	2 ± 1	0.9–15.7	9 ± 4
0.8 (<i>n</i> = 75)	0.9–5.9	3 ± 1	6.0–27.1	15 ± 5
0.66 (<i>n</i> = 75)	0.7–6.8	2 ± 1	2.2–12.1	6 ± 2
<i>Series 1, dialyzed</i>				
2.46 (<i>n</i> = 75)	0.7–6.0	3 ± 1	1.8–15.8	7 ± 4
<i>Series 2</i>				
0.8 (<i>n</i> = 85)	0.9–6.1	3 ± 1	5.5–29.6	15 ± 5
0.4 (<i>n</i> = 88)	0.7–7.2	3 ± 1	1.6–11.2	4 ± 2

sulted in particles with an apparent height of around 2 nm, and diameter of 3 nm (Table 4). The dialysis-stable iron–gluconate particles are thus slightly smaller than dialysis-stable iron–sucrose particles. In both cases, the dialyzed particle height (approximately 3 nm for iron–sucrose and 2 nm for iron–gluconate) is a good match for the iron mineral core diameter measured by TEM. The apparent widths of the dialyzed particles also show that the nanoparticle complexes, consisting of mineral cores and strongly bound carbohydrate, are slightly larger for iron–sucrose (7 nm) than for iron–gluconate (3–4 nm).

To better visualize the size of dialyzed iron–gluconate particles, some portion of the sample presented in Fig. 7(b) was centrifuged for 20 min at 27,200g to increase the concentration of iron beads in a unit volume. Fig. 7(c) represents the sample after centrifugation, from which it is apparent that the majority of the dialyzed particles are smaller than those in the image of the biggest dilution (Fig. 6(h)). Such a difference can be explained by the hypothesis that some carbohydrate in the original solution, which was associated with the surface of the iron–gluconate complex, was removed by dialysis. The difference in average height between the

sample at the greatest dilution and the dialyzed sample is 1 nm, and the difference in apparent diameter is nearly 8 nm (Table 3). That difference is proposed to arise from a layer of associated gluconate and/or sucrose, which is then susceptible to removal by dialysis. In contrast to our observations, Fishbane [29] has proposed that iron–gluconate is a stable iron complex with gluconate and sucrose that is unaffected by dilution or dialysis.

It is interesting to compare our AFM images of iron-carbohydrate complexes with published AFM studies of colloidal iron particles that have no bound carbohydrate. Stipp et al. have observed colloidal particles of ferrihydrite, hematite, goethite and lepidocrocite [30]. Those different polymorphs had significantly different AFM images: separated small spheres in the case of ferrihydrite, big aggregates for hematite, smooth separated rods for goethite and aggregates of rods for lepidocrocite. Vujtek et al. used AFM in the tapping mode to examine nanopowders of different iron oxides [31]. Since the samples were of powder character and not in solution, the authors observed extensive agglomeration on the mica surface. After dispersion of the powders in water and sonication, particles of hematite appeared as round beads with heights of 5–11 nm and diameter of

Table 4
AFM measurements of iron–gluconate at different dilutions and after dialysis

Fe Concentration (mg/mL)	Height range (nm)	Average height (nm)	Diameter range (nm)	Average diameter (nm)
<i>Series 1</i>				
5.00 (<i>n</i> = 75)	0.8–6.5	3 ± 1	3.8–25.4	12 ± 5
2.50 (<i>n</i> = 75)	0.7–4.1	2 ± 1	6.9–41.4	16 ± 7
0.83 (<i>n</i> = 75)	1.1–8.9	3 ± 2	3.4–20.4	11 ± 4
0.62 (<i>n</i> = 75)	0.9–7.8	3 ± 1	3.9–23.8	11 ± 4
<i>Series 1, dialyzed</i>				
2.7 (<i>n</i> = 75)	0.5–4.2	2 ± 1	1.1–6.9	3 ± 1
2.7 (<i>n</i> = 31)	0.5–4.1	2 ± 1	0.9–7.0	3 ± 1
<i>Series 2, dialyzed</i>				
N.D. (<i>n</i> = 73)	0.6–5.6	2 ± 1	2.7–9.6	4 ± 2

N.D., not determined.

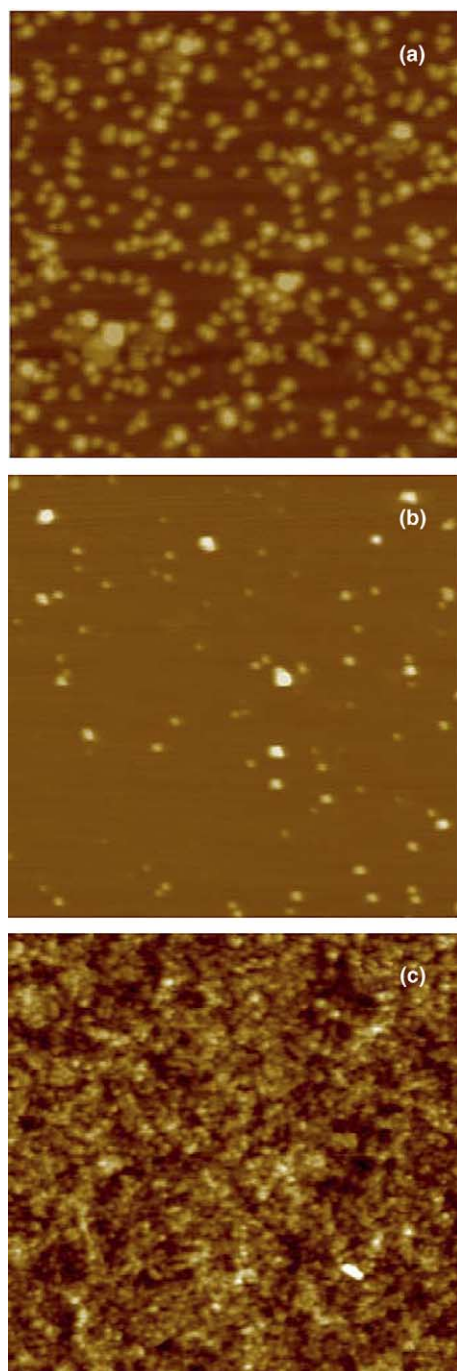


Fig. 7. Atomic force microscope height images of: (a) dialyzed iron-sucrose complex, (b) dialyzed iron-gluconate complex before centrifugation and (c) dialyzed iron-gluconate after concentration by centrifugation. Images size: $1\ \mu\text{m} \times 1\ \mu\text{m}$, with a color scale covering a height range of 8–15 nm.

30–80 nm (uncorrected for the finite width of the AFM tip). However, ferromagnetic iron oxides still exhibited some aggregation, which have been described as magnetic orientation on the mica surface caused by a magnetic holder for both sample and cantilever. On the other hand, Raşa and Philipse, in their AFM studies of magnetite particles by tapping mode, have never re-

Table 5

Elemental composition of dialyzed iron-sucrose and iron-gluconate		
	Iron-sucrose	Iron-gluconate
Total carbon (mg/L)	345	340
Iron (mg/L)	2290	2050
Sodium (mg/L)	<0.5	5.1
Fe/C (mol/mol)	1.45	1.30
C/Na (mol/mol)	–	130

ported any magnetic orientations [32]. Strongly ferromagnetic nanoparticles of magnetite appeared as small well-dispersed spheres of 6 nm height and 16 nm uncorrected diameter. The iron-carbohydrate nanoparticles examined in the present study appear to be smaller than the colloidal iron particle sizes previously reported.

3.5. Elemental analysis

The elemental composition of dialyzed samples is presented in Table 5. For the iron-sucrose complex, the molar ratio of Fe:C was 1.45:1. From this ratio, one sucrose molecule of 12 carbon atoms is present for 17 atoms of Fe.

If we assume that the iron core of iron-sucrose is a sphere 3.2 nm in diameter (the average from TEM measurements), then its volume would be $17.2\ \text{nm}^3$ and the surface area $32.2\ \text{nm}^2$. From the akaganeite JSPDS-ICDD reference card, one unit cell, containing 8 FeOOH, has a volume of $328\ \text{\AA}^3$. So, that sphere will consist of $17.2\ \text{nm}^3/0.328\ \text{nm}^3 = 52$ unit cells or 416 Fe atoms. From the molar ratio determined by elemental analysis (1.45:1), it will be surrounded by 287 atoms of carbon which corresponds to 24 sucrose molecules. In that case, one sucrose molecule will occupy $32.3/24 = 1.34\ \text{nm}^2$ of surface area on the mineral core. That area is slightly larger than the exposed surface of one akaganeite unit cell of $1\ \text{nm}^2$, which might thus involve about 6–8 surface Fe atoms. Based on this model, the corresponding total molecular mass of dialyzed iron-sucrose complex would be approximately 45 kDa. This estimate does not include an unmeasured content of Cl^- ions or loosely bound sucrose not retained by the complex after isolation by dialysis.

For the iron-gluconate complex, the elemental analysis gives the molar ratio of Fe:C as 1.30:1. If we consider a spherical model for the mineral core with 2 nm diameter, its volume would be $4.2\ \text{nm}^3$ and surface area $12.6\ \text{nm}^2$. Considering the volume of an akaganeite unit cell ($0.328\ \text{nm}^3$), that particle will contain 102 Fe atoms. If we assume that the carbohydrate shell remaining after dialysis is solely composed of gluconate, the above molar ratio will give us about 13 gluconate molecules. In that case, the surface area available for one gluconate molecule will be $0.97\ \text{nm}^2$. The corresponding total molecular mass would be approximately 11.6 kDa. This estimate does not include an unmeasured content of Cl^-

ions or loosely bound sucrose not retained by the complex after isolation by dialysis.

The elemental composition also showed a low level of sodium in iron–gluconate. The molar ratio of C to Na was 130:1. This ratio corresponds to one sodium ion per 21 gluconate molecules. This low level of Na is likely to represent a residual monovalent counterion accompanying the charged particle through dialysis by nonspecific ion–polyelectrolyte interactions.

The apparent molecular masses cited above are subject to some uncertainty. First, it should be stressed that elemental analysis data could only be obtained for dialyzed samples, and that loosely associated carbohydrate is lost during dialysis. In addition, the calculation is highly sensitive to our estimate of the mineral core diameter for dialyzed samples. The average diameters used for each preparation were established primarily by TEM measurements, and supported by the AFM height measurements. The X-ray diffraction data give similar values, but with a somewhat smaller difference between iron–sucrose and iron–gluconate. In fact, the core diameters measured by TEM and AFM height are not statistically significantly different. The elemental analyses are also very similar. Thus, the cores sizes and the formula weights for the two preparations may be equal within experimental uncertainty.

4. Summary

Analysis of two parenteral iron formulations indicates that the electronic environment of the iron is consistent with a polynuclear iron oxyhydroxide core structure, stabilized by interaction with carbohydrate. The core particles are composed of iron oxyhydroxide in the β -FeOOH mineral polymorph known as akaganeite. The core particles have Cl^- ions present in channels of the porous akaganeite structure. Atomic force microscopy and transmission electron microscopy show the presence of nanoparticles of fairly uniform size for a given preparation.

A model for the average iron–sucrose particle, based on analyses of particles after removal of loosely bound carbohydrate by dialysis, is a core of ferric oxyhydroxide in the akaganeite β -FeOOH polymorph, with an approximate diameter of 3 nm, with a layer of attached sucrose molecules, forming a particle with a final diameter of about 7 nm. Assuming a roughly spherical shape, the average core particle has about 416 FeOOH. Based on the elemental analysis, the average core particle is surrounded by about 24 sucrose molecules. Based on this data, the corresponding apparent molecular mass of iron–sucrose complex would be approximately 45 kDa.

A model for the average iron–gluconate particle, based on analyses of particles after removal of loosely bound carbohydrate by dialysis, is a core composed of a 2 nm diameter akaganeite core, with a thin shell of gluconate. Assuming a roughly spherical particle shape, the average core particle has about 102 FeOOH units. Based on the elemental analysis, the average core particle is surrounded by about 13 gluconate molecules. The corresponding apparent molecular mass is approximately 11.6 kDa.

For both iron–sucrose and iron–gluconate, the particles as present in the formulations before dialysis are larger, as a result of weak association of additional carbohydrates. Thus the effective size of the particles when used therapeutically will depend on the degree of dilution experienced and the rate of carbohydrate dissociation under the conditions of use.

Acknowledgements

This research was supported by American Regent, Inc. A. Ulman and J.L. acknowledge the support from the NSF Garcia MRSEC for Polymers at Engineered Interfaces.

References

- [1] W. Schneider, B. Schwyn, in: W. Stumm (Ed.), *Aquatic Surface Chemistry: Chemical Processes at the Particle–Water Interface*, Wiley, New York, 1987, pp. 167–196.
- [2] W. Schneider, *Chimia* 42 (1988) 9–20.
- [3] R.M. Cornell, U. Schwertmann, *The Iron Oxides*, VCH Verlagsgesellschaft mbH, Weinheim, 2003.
- [4] B. Gyurcsik, L. Nagy, *Coord. Chem. Rev.* 203 (2000) 81–149.
- [5] G. Bates, J. Hegenauer, J. Renner, P. Saltman, T.G. Spiro, *Bioinorg. Chem.* 2 (1973) 311–327.
- [6] L. Nagy, A. Szorcsik, *J. Inorg. Biochem.* 89 (2002) 1–12.
- [7] E. Ferrari, M. Saladini, *J. Inorg. Biochem.* (2004), published online March 18.
- [8] P.R. Marshall, D. Rutherford, *J. Colloid. Interface Sci.* 37 (2) (1971) 390–402.
- [9] J.S.G. Cox, G.R. Kennedy, J. King, P.R. Marshall, D. Rutherford, *J. Pharm. Pharmac.* 24 (1972) 513–517.
- [10] L. Piceni-Sereni, T. Mereu, *Minerva Pediatrica* 45 (1961) 1533–1538.
- [11] I. Minoli, *Gazzetta Medica Italiana* (1962) 121.
- [12] A. Müller, *Drug Research.* 17 (1967) 921–931.
- [13] E.M. Coe, L.H. Bowen, R.D. Bereman, J.A. Speer, W.T. Monte, L. Scaggs, *J. Inorg. Biochem.* 57 (1995) 63–71.
- [14] E.M. Coe, L.H. Bowen, J.A. Speer, Z. Wang, D.E. Sayers, R.D. Bereman, *J. Inorg. Biochem.* 58 (1995) 269–278.
- [15] S.H. Kilcoyne, A. Gorisek, *J. Magn. Magn. Mat.* 177–181 (1998) 1457–1458.
- [16] B. Knight, L.H. Bowen, R.D. Bereman, S. Huang, E. DeGrave, *J. Inorg. Biochem.* 73 (1999) 227–233.
- [17] F. Jones, H. Cölfen, M. Antonietti, *Colloid Polym. Sci.* 278 (2000) 491–501.
- [18] F. Jones, H. Cölfen, M. Antonietti, *Biomacromolecules* 1 (2000) 556–563.

- [19] K. Geetha, M.S.S. Raghavan, S.K. Kulshreshtha, R. Sasikala, C.P. Rao, *Carb. Res.* 271 (1995) 163–175.
- [20] M.I. Oshtrakh, V.A. Semionkin, P.G. Prokopenko, O.B. Milder, A.B. Livshits, A.A. Kozlov, *Int. J. Biol. Macromol.* 29 (2001) 303–314.
- [21] R. Lawrence, *PDA J. Pharm. Sci. Technol.* 52 (1998) 190–197.
- [22] F. Funk, G.J. Long, D. Hautot, R. Büchi, I. Christl, P.G. Weidler, *Hyperfine Interactions* 136 (2001) 73–95.
- [23] J.I. Langford, A.J.C. Wilson, *J. Appl. Crystallogr.* 11 (1978) 102–113.
- [24] E. Margeat, C. Le Grimellac, C.A. Royer, *Biophys. J.* 75 (1998) 2712–2720.
- [25] E. Farkas, É.A. Enyedy, L. Zékány, G. Deák, *J. Inorg. Biochem.* 83 (2–3) (2001) 107–114.
- [26] A.C. Scheinost, U. Schwertmann, *Soil Sci. Soc. Am. J.* 63 (1999) 1463–1471.
- [27] A.C. Scheinost, A. Chavernas, V. Barrón, J. Torrent, *Clays Clay Miner.* 46 (1998) 528–536.
- [28] N.D. Chasteen, P.M. Harrison, *J. Struct. Biol.* 126 (1999) 182–194.
- [29] S. Fishbane, *Am. J. Kidney Diseases* 41 (2003) S18–S26.
- [30] S.L.S. Stipp, M. Hansen, R. Kristensen, M.F. Hochella Jr., L. Bennedsen, K. Dideriksen, T. Balic-Zunic, D. Léonard, H.-J. Mathieu, *Chem. Geol.* 190 (2002) 321–337.
- [31] M. Vujtek, R. Zboril, R. Kubinek, M. Mashlan, *Chem. Mater.* 14 (2002) 969–977.
- [32] M. Raşa, A.P. Philipse, *J. Magn. Magn. Mater.* 252 (2002) 101–103.